Contribution of Fe 3*d* states to the Fermi level of $CaFe_2As_2$

E. Z. Kurmaev,[1] J. A. McLeod,[2,*] A. Buling,[3] N. A. Skorikov,[1] A. Moewes,[2] M. Neumann,[3] M. A. Korotin,[1] Yu. A. Izyumov,[1] N. Ni,[4] and P. C. Canfield[4]

[1]*Institute of Metal Physics, Russian Academy of Sciences-Ural Division, 620219 Yekaterinburg, Russia*

[2]*Department of Physics and Engineering Physics, University of Saskatchewan, 116 Science Place, Saskatoon, Saskatchewan, Canada S7N 5E2*

[3]*Department of Physics, University of Osnabrück, Barbarastr. 7, D-49069 Osnabrück, Germany*

[4]*Ames Laboratory, Department of Physics and Astronomy and U.S. DOE, Iowa State University, Ames, Iowa 50011, USA*

(Received 29 January 2009; revised manuscript received 20 July 2009; published 7 August 2009)

We present density functional theory (DFT) calculations and soft x-ray spectra (soft x-ray spectroscopy and x-ray photoelectron spectra) measurements of single-crystal $CaFe_2As_2$. The experimental valence-band spectra are consistent with our DFT calculations. Both theory and experiment show that the Fe 3*d* states dominate the Fermi level and hybridize with Ca 3*d* states. The simple shape of x-ray photoelectron Fe 2*p* core level spectrum (without any satellite structure typical for correlated systems) suggests that the Fe 3*d* electrons are weakly or at most moderately correlated.

DOI: 10.1103/PhysRevB.80.054508 PACS number(s): 74.70.−b, 78.70.En, 71.15.Dx

I. INTRODUCTION

Soon after finding superconductivity in the *R*OFeAs (*R* rare earth) compounds,[1] the $AEFe_2As_2$ (*AE*=Ca, Sr, Ba, Eu) family of Fe-As superconductors with a $ThCr_2Si_2$-type tetragonal structure (space group I4/mmm) was discovered.[2,3] A structural phase transformation from a high-temperature tetragonal phase to a low-temperature orthorhombic phase occurs in these compounds between 140 and 170 K.[2,3] Although these materials are not superconducting at ambient pressure, superconductivity can be achieved by doping the *AE* and Fe sites[2,4–6] or by applying high pressure.[7–9] In both cases superconductivity can only occur when the phase transformation from tetragonal to orthorhombic structure can be easily realized or when it is fully suppressed. A similar structural phase transition also appears in the *R*OFeAs compounds and is likewise suppressed by *F* doping,[1] which strongly links the superconductivity of doped iron arsenides to the proximity to this structural instability of $AEFe_2As_2$ compounds and possibly to the spin-density wave ordering.[10–12] However the phase transformation in $CaFe_2As_2$ does not have a significant effect on the density of states.[13]

The calculated electronic structures of $BaFe_2As_2$ (Ref. 14) and LaOFeAs (Ref. 15) are similar, and the bands around the Fermi level for both compounds are mainly formed by Fe 3*d* states; the difference in the valence band of both compounds is observed only in the noniron states. In the LaOFeAs system, As 4*p* states hybridize with O 2*p* states and separate from the Fe 3*d* bands whereas in $BaFe_2As_2$ the Fe 3*d* and As 4*p* states hybridize. Similar results are found from other density functional theory (DFT) calculations.[6,14,16] In this respect the study of the electronic structure of $CaFe_2As_2$ is of particular interest because Ca 3*d* states can interact with Fe 3*d* states and therefore modify the distribution of Fe 3*d* states near the Fermi level. Another point of interest is the strength of the Fe 3*d* electron correlations. Recently it has been proposed that the related compound, LiFeAs,[17] is strongly correlated with significant on-site Coulomb interactions. To contrast, earlier experimental investigations of LaOFeAs (Ref. 18) report the same high-spin state configuration of Fe, but conclude that the system is at most moderately correlated. A detailed study of the electronic states in $CaFe_2As_2$ is of interest in this ongoing debate, since $CaFe_2As_2$ represents yet another subfamily of the FeAs superconducting materials.

We have studied both iron and calcium resonant and nonresonant $L_{2,3}$ x-ray emission spectra (XES), which probe the occupied partial Fe 3*d* and Ca 3*d* densities of states (DOS). We compare them with x-ray photoemission spectroscopy (XPS) valence-band measurements (which probe the total occupied DOS) and our full potential linearized augmented plane-wave (FP-LAPW) electronic structure calculations of $CaFe_2As_2$.

II. EXPERIMENTAL AND CALCULATION DETAILS

Single crystals of $CaFe_2As_2$ were grown out of a Sn flux using conventional high-temperature solution growth techniques in experimental conditions described in Refs. 3 and 19. Elemental Ca, Fe, and As were added to Sn in the ratio of $CaFe_2As_2$:Sn=1:48 and placed in a 2-ml alumina crucible. A second catch crucible containing silica wool was placed on top of the growth crucible and sealed in a silica ampoule under approximately 1/3 atmosphere pressure of argon gas. The sealed ampoule was placed in a programmable furnace and heated to 850 °C and cooled over 36 h to 500 °C. The high quality of the $CaFe_2As_2$ crystals was confirmed by an extensive characterization employing x-ray diffraction, neutron diffraction, and thermodynamic and transport techniques.[10,19]

XPS measurements were obtained using a Perkin-Elmer PHI 5600 ci Multitechnique system with monochromatized Al Kα radiation (with a full width at half-maximum of 0.3 eV). The energy resolution of the spherical capacitor analyzer was adjusted to approximately ΔE=0.45 eV. The pressure in the ultrahigh-vacuum chamber was in the 10^{-10} mbar range during the measurements. The $CaFe_2As_2$ crystal was

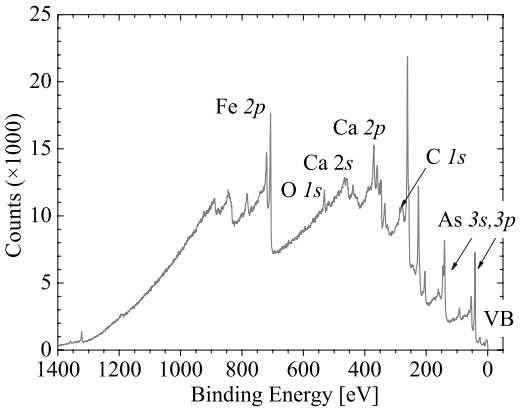

FIG. 1. XPS survey spectrum of $CaFe_2As_2$.

cleaved *in situ*. The surface contamination was monitored with O 1*s* and C 1*s* core-level spectra before and after our measurements. In addition, the XPS survey spectrum (see Fig. 1) demonstrates a low level of oxygen and carbon contamination and therefore their negligible contribution to the valence-band spectrum.

The resonant and nonresonant x-ray emission measurements of $CaFe_2As_2$ were performed at the soft x-ray fluorescence endstation of Beamline 8.0.1 at the Advanced Light Source in the Lawrence Berkeley National Laboratory.[20] The endstation uses a Rowland circle geometry x-ray spectrometer with spherical gratings and an area sensitive multichannel detector. We have measured the resonant and nonresonant Fe $L_{2,3}$ ($3d,4s \rightarrow 2p$ transition) and nonresonant Ca $L_{2,3}$ ($3d,4s \rightarrow 2p$ transition) x-ray emission spectroscopy. The instrument resolving power ($E/\Delta E$) for emission measurements was 10^3. All spectra were normalized to the incident photon current using a highly transparent gold mesh in front of the sample to measure the intensity fluctuations in the photon beam. To identify energies for resonant emission, and for sake of completeness, we measured x-ray absorption spectroscopy (XAS) for both Fe 2*p* and Ca 2*p* electrons. XAS probes the unoccupied partial DOS (the conduction band), but for transition metals the spectra are severely distorted by the presence of the 2*p* core hole, and therefore XAS spectra are not very useful for our current analyses. XAS measurements for Fe were taken with total fluorescence yield (TFY) and total electron yield (TEY) modes. Self-absorption in $L_{2,3}$ spectra of transition metals is significant, which suppresses features in TFY XAS. However, since we used the XAS measurements primarily to identify resonant energies for XES, the TFY spectra were useful as they reduce surface oxidation effects that can cause shifts in spectral features. The instrumental resolving power ($E/\Delta E$) for absorption measurements was about 2×10^3. The chosen excitation energies for XES corresponded to the locations of the L_3 and L_2 thresholds, an energy just above each threshold, and one energy well above resonance.

All partial DOS calculations were performed within the FP-LAPW method as implemented in the WIEN2K code.[21] For the exchange-correlation potential we used the Perdew-Burke-Ernzerhof gradient approximation variant (GGA).[22] The calculation model was non-magnetic, and spin polarization was not considered. The Brillouin zone integrations were performed with a $11 \times 11 \times 11$ special *k*-point grid and $R_{MT}^{\min} K_{\max} = 7$ (the product of the smallest of the atomic sphere radii R_{MT} and the plane-wave cutoff parameter $K_{\max}$) was used for the expansion of the basis set. The experimentally determined lattice parameters of the high-temperature phase of $CaFe_2As_2$ ($a = 3.912$ Å, $c = 11.667$ Å) (Ref. 19) were used in our calculations. We chose the *z* parameter of As in $BaFe_2As_2$ (Ref. 14) as a starting approximation and performed structural relaxation calculations on the As *z* parameter to minimize internal forces. The resulting coordinates of As were (0.0, 0.0, 0.35814). Atomic sphere radii of $R_{Ca} = 2.5$, $R_{Fe} = 2.17$, and $R_{As} = 1.92$ a.u. were chosen in the FP-LAPW calculation. These were selected so that the spheres are nearly touching. For comparison, we also performed FP-LAPW band-structure calculations for $BaFe_2As_2$ using the manner outlined in Ref. 14.

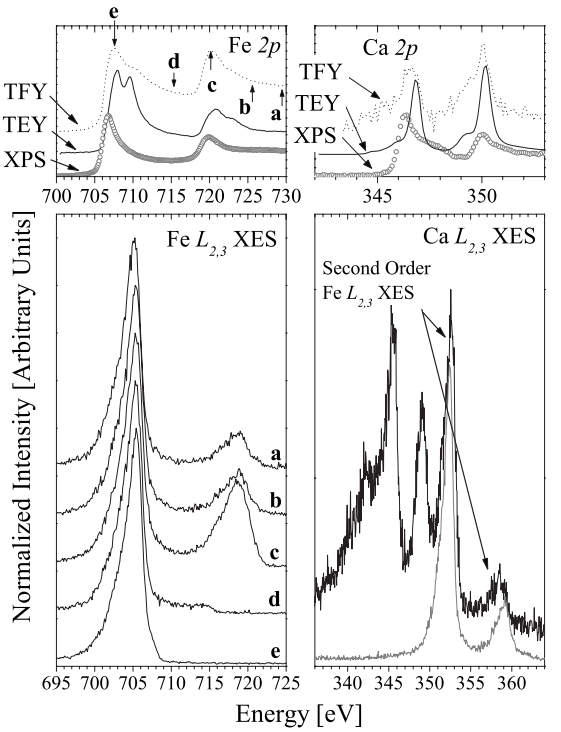

FIG. 2. Summary of spectra for $CaFe_2As_2$. Left panels show the Fe $L_{2,3}$ spectra, right panels the Ca $L_{2,3}$ spectra. Excitation energies for Fe $L_{2,3}$ XES are indicated by arrows in the TFY spectra in the top left panel. Note the presence of second-order Fe $L_{2,3}$ appearing in the Ca $L_{2,3}$ XES; the Fe $L_{2,3}$ nonresonant XES (curve a in the left panel) at half the normal energy scale has been replotted here in gray.

III. RESULTS AND DISCUSSION

The measured XES, XAS, and XPS spectra are shown in Fig. 2. The XPS Fe 2*p* core-level spectrum (Fig. 2, top left panel) lacks the satellite structure typical for correlated systems (for instance for FeO) (Ref. 23) and the Fe $2p_{3/2}$ peak is sharp and similar to metallic iron.[24] A similar simple shape of Fe 2*p* XPS is observed for LaOFeAs.[25] This supports the postulate that in these FeAs-based systems the Fe 3*d* elec-

trons are not strongly correlated. The Fe $L_{2,3}$ XES (Fig. 2, bottom left panel) indicate two main bands located around 705 and 718 eV correspond to the Fe L_3 ($3d4s \rightarrow 2p_{3/2}$ transitions) and Fe L_2 ($3d4s \rightarrow 2p_{1/2}$ transitions) normal-emission lines separated by the spin-orbital splitting of Fe 2*p* states. The resonant XES spectra (XES curves b, c, d, and e in bottom left panel of Fig. 2) show no energy-loss features; this indicates that Fe $L_{2,3}$ XES of $CaFe_2As_2$ probes mainly the partial DOS. The Fe L_3 XES do not show any features that would indicate the presence of a lower Hubbard band or a sharp quasiparticle feature that was previously predicted by LDA+DMFT analysis,[26] suggesting that LDA+DMFT might not be the correct approach to calculating the electronic structure of this system. The Ca XES (Fig. 2, bottom right panel) shows the spin-orbital splitting of Ca 2*p* states. Unfortunately, the Ca XES is distorted significantly by the second-order XES from Fe $L_{2,3}$. The small spin-orbit splitting and low fluorescent yield (notice that the Ca $L_{2,3}$ XES has more noise than the Fe $L_{2,3}$ XES) of Ca combined with the distortion of the second-order Fe emission complicates the analysis of these spectra.

The nonresonant Fe $L_{2,3}$ XES of LaOFeAs and $CaFe_2As_2$ have almost identical ratios in the integral intensity of the L_2 and L_3 peaks [the $I(L_2)/I(L_3)$ ratio]. For free atoms the relative intensity ratio of L_2 and L_3 XES lines is determined only by the statistical population of $2p_{1/2}$ and $2p_{3/2}$ levels and therefore should be equal to $\frac{1}{2}$. In metals the radiationless $L_2L_3M_{4,5}$ Coster-Kronig (C-K) transitions strongly reduce the $I(L_2)/I(L_3)$ ratio[27] and therefore the $I(L_2)/I(L_3)$ ratio is a measure for the metallicity of transition-metal compounds.[28] The intensity ratios shown in Fig. 3 for LaOFeAs and $CaFe_2As_2$ are closer those of metallic Fe than those of the strongly correlated FeO. This further supports our conclusion that the Fe 3*d* states in FeAs systems are weakly or at most moderately correlated.

To assist in the interpretation of the experimental data, GGA calculations were performed. The calculated electronic structure of $CaFe_2As_2$ and $BaFe_2As_2$ are shown in Fig. 4. The As 4*s* states are concentrated at the bottom of the valence band (~−11.2 eV). The As 4*p*-like band shows a two-peak structure (at ~−5.2 and −3.3 eV) and the upper band is a mixture of Fe 3*d* and Ca 3*d* states or Ba 5*d* states. The top of the valence band (−1–0 eV) is formed by Fe 3*d* and Ca 3*d* states or Ba 5*d* states with the main spectral weight centered at −0.48 eV. Fe 3*d* states dominate at the Fermi level, similar to the situation for the Fermi level of LaOFeAs.[15,29,30] The Fe 3*d* states hybridize with As 4*p* states located around −4–3 eV below the Fermi level. Note that the position and shape of Fe 3*d* DOS are nearly identical for both compounds and are not altered when Ca replaces Ba. The Ca 3*d* states or Ba 5*d* states have only a minor contribution (~5%) to the DOS near the Fermi level and are strongly mixed with the Fe 3*d* states and As 4*p* states. The Fe and Ca 4*s* states and Ba 6*s* states have negligible contribution to the valence DOS. From the band-structure calculations of $CaFe_2As_2$ and the comparison with those for LaOFeAs we conclude that the FeAs layer in both systems determines the main features of their energy bands. In both cases the Fe 3*d* states provide the main contribution to the DOS near the Fermi level.

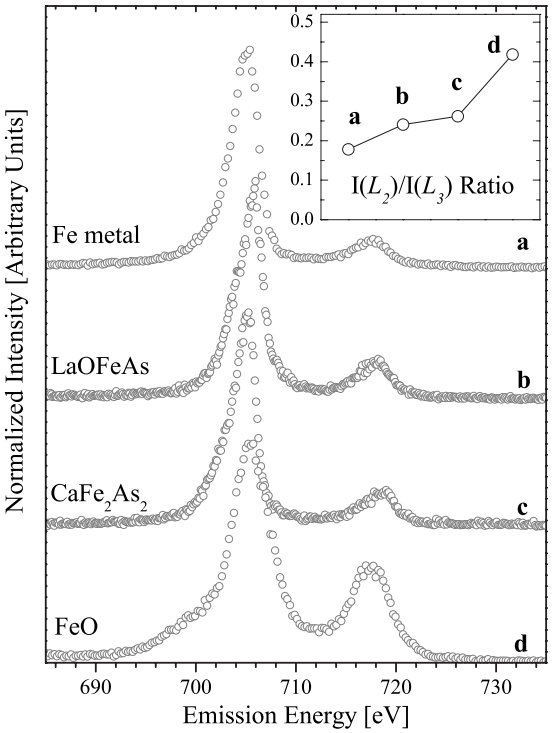

FIG. 3. Fe $L_{2,3}$ XES spectra and comparison of the $I(L_2)/I(L_3)$ ratios (inset) for metallic Fe, LaOFeAs, $CaFe_2As_2$, and correlated FeO. The $I(L_2)/I(L_3)$ was calculated from the ratios of the integral under the L_2 and L_3 peaks, respectively.

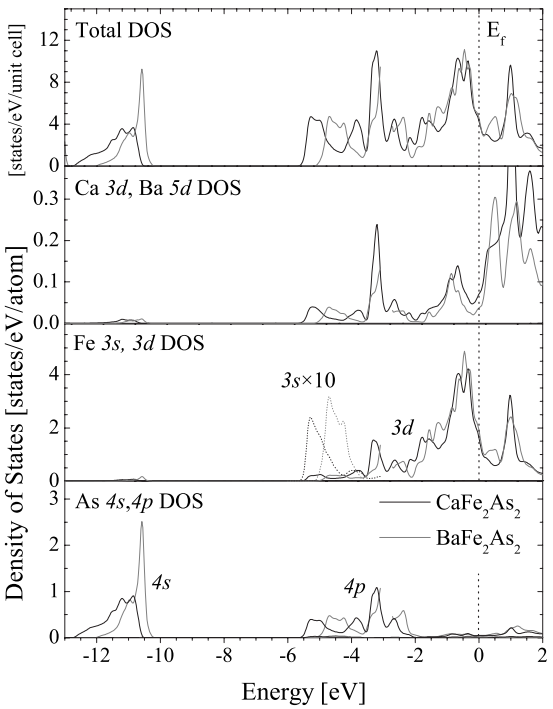

FIG. 4. Calculated DOS for $CaFe_2As_2$ and $BaFe_2As_2$. The dotted lines in the Fe 3*s*, 3*p* DOS plot refer to the 3*s* states increased by a factor of 10. The *y* axis in the total DOS plot is in units of [states/eV/unit cell].

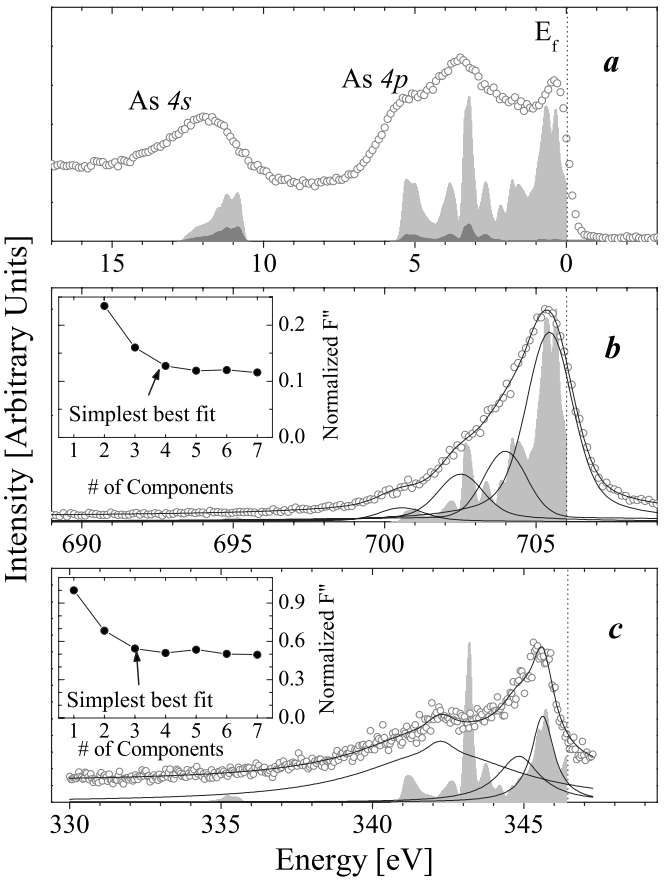

FIG. 5. Comparison of calculated DOS and measured spectra. (a) XPS VB spectra and total DOS (light gray, proportional to [states/eV/unit cell]), the As 4*s*, 4*p* DOS (dark gray, proportional to [states/eV/atom]). (b) Fe L_3 peak of $L_{2,3}$ spectra, Fe 3*d* DOS, best-fit curve, and the four pseudo-Voigt components contributing to the best-fit curve. (c) Ca L_3 peak of $L_{2,3}$ spectra, Ca 3*d* DOS, best-fit curve, and the three pseudo-Voigt components contributing to the best-fit curve. The insets on (b) and (c) show the normalized fit parameter F'' (note that the "worst" fit has a normalized F'' of 1.0, for 1 component in Fe this is off the scale of the plot) for fits with different numbers of pseudo-Voigt components. The estimated Fermi level is indicated in each plot.

The XPS valence-band (VB) measurements of $CaFe_2As_2$ show four distinct sub-bands located at ~−11.9, −5.1, −3.4, and −0.4 eV. The binding energies of these subbands are in excellent agreement with the calculated partial DOS (Fig. 5(a)). We also note that the XPS VB of $CaFe_2As_2$ is in agreement with photoemission measurements of $LaFeAsO_{1x}F_x$ ($x=0,0.06$).[25] Neglecting small differences due to the contribution of O 2*p* states in $LaFeAsO_{1x}F_x$, the overall picture of the XPS VB near the Fermi level is very similar for both compounds and mainly determined by Fe 3*d* states.

The $L_{2,3}$ XES spectra were analyzed by curve fitting for both Ca and Fe. Since the L_2 XES peak is the same shape as the L_3 XES but with poorer statistics, only the L_3 XES peak was fitted. Least-squares fitting was applied to a superposition of pseudo-Voigt functions (of the form listed in Eq. (1)).

$$f_V = A[\eta f_G + (1-\eta) f_L]$$

$$f_G = \frac{1}{\sqrt{2\pi}\sigma}\exp\left(-\frac{(x-\mu)^2}{2\sigma^2}\right)$$

$$f_L = \frac{1}{\pi}\left(\frac{\frac{\Gamma}{2}}{(x-\mu)^2+\left(\frac{\Gamma}{2}\right)^2}\right). \quad (1)$$

Each L_3 XES spectra was fitted with a number of pseudo-Voigt functions. The mixing-factor η was consistent for each pseudo-Voigt function in the fit. In addition to η, each component had the position μ_i, Lorentzian broadening Γ_i, and peak amplitude A_i determined by least-squares fitting. The Gaussian broadening, σ, was fixed at the instrumental energy resolution—that is, the peak center μ_i divided by the resolving power $E/\Delta E$. The number of pseudo-Voigt components for each spectra was varied from one to seven. The fit quality parameter $F''=\sqrt{\Sigma_x[f_{\text{data}}(x)-f_{\text{fit}}(x)]^2}$ was used to choose the "simplest, best" fit—the minimum number of components which produce a consistent F'' (see insets in Figs. 5(a) and 5(b)). In short; we fitted n pseudo-Voigt components to the L_3 XES spectrum (for $1 \le n \le 7$) and examined the F'' parameter to find the fewest number of components that produced a good fit. We should point out that the fits were fairly insensitive to the guesses for the initial positions μ_i (for example, any location between about 700 and 707 eV for Fe L_3 XES is a reasonable initial position) and extremely insensitive to the guesses for the initial values of the remaining parameters (η, A_i, and Γ_i). Only the number of pseudo-Voigt functions chosen had a strong effect on the quality of the fit, so the position and shape of the components is relatively free of bias. For fitting the Fe L_3 XES spectrum four or more components produced fits with F'' values that were equal within 10%, whereas the F'' for three components was ~25% greater than the F'' for four components. For fitting the Ca L_3 XES spectrum three or more components produced fits with F'' values that were equal within 10%, whereas the F'' for two components was ~26% greater than the F'' for three components. This suggests that the Fe and Ca L_3 XES spectra are composed of at least four and three bands, respectively. The results from fitting are summarized in Table I.

The pseudo-Voigt components for the Fe L_3 XES (see Fig. 5(b)) have roughly the same position and proportional amplitude as the main energy-separated features in the Fe 3*d* DOS. The agreement between the calculated Fe 3*d* DOS and the measured Fe L_3 XES further supports the conclusion that the valence band of $CaFe_2As_2$ is dominated by weakly correlated 3*d* Fe electrons. The pseudo-Voigt components for the Ca L_3 XES (see Fig. 5(c)) do not agree as well with the calculated Ca 3*d* DOS as did Fe. However, the effect of core-hole broadening increases as the square of the distance from the top of the valence band,[31] the Ca XES is of generally lower-quality compared to that of Fe, and the narrow spin-orbit separation in Ca provides a very small pre-edge region (essential in determining the correct spectral background for curve fitting). It is therefore not unexpected we could not resolve postedge features clearly. The poor quality of the Ca L_3 XES spectra and the almost overwhelming influence

TABLE I. Fit results for the four pseudo-Voigt peaks for fitting the Fe L_3 XES and three pseudo-Voigt peaks for fitting the Ca L_3 XES. Note there is only one mixing-factor η for all Fe components and one for all Ca components.

	Fe_1	Fe_2	Fe_3	Fe_4	Ca_1	Ca_2	Ca_3
η_i	0.50				0.02		
A_i	2.39	1.09	0.64	0.18	0.73	0.74	3.03
μ_i (eV)	705.4	703.98	702.5	700.6	345.6	344.8	342.2
Γ_i (eV)	3.60	15.97	4.83	3.71	0.91	1.78	6.17

of second-order Fe L_3 XES indicate that Ca 3*d* electrons contribute far less to the valence-band DOS than Fe 3*d* electrons.

The Fermi levels for the Ca and Fe L_3 XES spectra in Fig. 5 were estimated by aligning the calculated DOS with the fitted pseudo-Voigt components, so the agreement between DOS and the first pseudo-Voigt component is manufactured. Other methods of estimating the Fermi level in XES spectra involve using the peak of the second derivative in the XES,[32] or the metal 2*p* binding energy from XPS data.[33] For the Fe L_3 XES spectrum the Fermi level is estimated at 706.0, 706.8, and 706.9 eV by aligning DOS and fit components, using the binding energy of Fe 2*p* XPS, and using the peak in the second derivative of the Fe L_3 XES spectra, respectively. For the Ca L_3 spectrum the Fermi level is estimated at 346.4, 346.3, and 346.3 eV by aligning DOS and fit components, using the binding energy of Ca 2*p* XPS, using the peak in the second derivative of the Ca L_3 XES. The agreement in estimated Fermi levels for the Fe L_3 XES is not as good as that for the Ca L_3 XES. However, the occupancy of the Fe 3*d* states suffer a more abrupt cut-off at the Fermi level than the Ca 3*d* states. This suggests that the Fe L_3 XES potion at higher energies than the main peak at 705.4 eV is due only to spectral broadening. It is therefore not unexpected that the XPS 2*p* binding energy and XES second-derivative estimates of the Fermi level are greater than the curve-fit alignment Fermi level estimate by a shift in roughly the instrumental broadening.

To summarize, we have performed a combined theoretical and experimental study of the electronic structure of $CaFe_2As_2$. Band structure calculations, experimental valence-band spectra, and core-level spectra show that the Fe 3*d* states dominate at the Fermi level and are very similar to those of LaOFeAs. While the Ca 3*d* states are completely hybridized with the Fe 3*d* states, the main spectral weight of Ca 3*d* states is at −0.48 eV below the Fermi level and there is only a minimal contribution (~5% of total states) at the Fermi level. From our experimental and theoretical evidence, we conclude that the Fe 3*d* states are weakly or at most moderately correlated.

ACKNOWLEDGMENTS

We acknowledge support of the Research Council of the President of the Russian Federation (Grant Nos. NSH-1929.2008.2 and NSH-1941.2008.2), the Russian Science Foundation for Basic Research (Project No. 08-02-00148), the Natural Sciences and Engineering Research Council of Canada (NSERC), and the Canada Research Chair program. P.C.C. acknowledges useful discussions with S. L. Bud'ko and G. D. Samolyuk. Work at the Ames Laboratory was supported by the Department of Energy, Basic Energy Sciences under Contract No. DE-AC02-07CH11358.

*john.mcleod@usask.ca

[1] Y. Kamihara, T. Watanabe, M. Hiranoand, and H. Hosono, J. Am. Chem. Soc. **130**, 3296 (2008).
[2] M. Rotter, M. Tegel, D. Johrendt, I. Schellenberg, W. Hermes, and R. Pöttgen, Phys. Rev. B **78**, 020503(R) (2008).
[3] N. Ni, S. L. Bud'ko, A. Kreyssig, S. Nandi, G. E. Rustan, A. I. Goldman, S. Gupta, J. D. Corbett, A. Kracher, and P. C. Canfield, Phys. Rev. B **78**, 014507 (2008).
[4] G. Wu, H. Chen, T. Wu, Y. L. Xie, Y. J. Yan, R. H. Liu, X. F. Wang, J. J. Ying, and X. H. Chen, J. Phys.: Condens. Matter **20**, 422201 (2008).
[5] C. Gen-Fu, Z. Li, G. Li, W. Z. Hu, J. Dong, X. D. Zhang, P. Zheng, N. L. Wang, and J. L. Luo, Chin. Phys. Lett. **25**, 3403 (2008).
[6] A. S. Sefat, R. Jin, M. A. McGuire, B. C. Sales, D. J. Singh, and D. Mandrus, Phys. Rev. Lett. **101**, 117004 (2008).
[7] M. S. Torikachvili, S. L. Bud'ko, N. Ni, and P. C. Canfield, Phys. Rev. Lett. **101**, 057006 (2008).
[8] T. Park, E. Park, H. Lee, T. Klimczuk, E. D. Bauer, F. Ronning, and J. D. Thompson, J. Phys.: Condens. Matter **20**, 322204 (2008).
[9] P. Alireza, Y. Chris Ko, J. Gillett, C. Petrone, J. Cole, G. Lonzarich, and S. Sebastian, J. Phys.: Condens. Matter **21**, 012208 (2009).
[10] A. I. Goldman, D. N. Argyriou, B. Ouladdiaf, T. Chatterji, A. Kreyssig, S. Nandi, N. Ni, S. L. Budko, P. C. Canfield, and R. J. McQueeney, Phys. Rev. B **78**, 100506(R) (2008).
[11] A. I. Goldman *et al.*, Phys. Rev. B **79**, 024513 (2009).
[12] H. Lee, E. Park, T. Park, V. A. Sidorov, F. Ronning, E. D. Bauer, and J. D. Thompson, Phys. Rev. B **80**, 024519 (2009).
[13] T. Yildirim, Phys. Rev. Lett. **102**, 037003 (2009).
[14] I. R. Shein and A. L. Ivanovskii, JETP Lett. **88**, 107 (2008).

[15] I. A. Nekrasov, Z. V. Pchelkina, and M. V. Sadovskii, JETP Lett. **88**, 155 (2008).
[16] D. J. Singh, Phys. Rev. B **78**, 094511 (2008).
[17] L. Hozoi and P. Fulde, Phys. Rev. Lett. **102**, 136405 (2009).
[18] T. Kroll *et al.*, Phys. Rev. B **78**, 220502(R) (2008).
[19] N. Ni, S. Nandi, A. Kreyssig, A. I. Goldman, E. D. Mun, S. L. Bud'ko, and P. C. Canfield, Phys. Rev. B **78**, 014523 (2008).
[20] J. J. Jia *et al.*, Rev. Sci. Instrum. **66**, 1394 (1995).
[21] P. Blaha, K. Schwarz, G. K. H. Madsen, D. Kvasnicka, and J. Luitz, WIEN2K, *An Augmented Plane Orbitals Program for Calculating Crystal Properties* (Technische Universität Wien, Austria, 2001).
[22] J. P. Perdew, K. Burke, and M. Ernzerhof, Phys. Rev. Lett. **77**, 3865 (1996).
[23] V. R. Galakhov, A. I. Poteryaev, E. Z. Kurmaev, V. I. Anisimov, S. Bartkowski, M. Neumann, Z. W. Lu, B. M. Klein, and T.-R. Zhao, Phys. Rev. B **56**, 4584 (1997).
[24] X. Gao, D. Qi, S. C. Tan, A. T. S. Wee, X. Yu, and H. O. Moser, J. Electron Spectrosc. Relat. Phenom. **151**, 199 (2006).
[25] W. Malaeb *et al.*, J. Phys. Soc. Jpn. **77**, 093714 (2008).
[26] K. Haule, J. H. Shim, and G. Kotliar, Phys. Rev. Lett. **100**, 226402 (2008).
[27] S. Raghu, X.-L. Qi, C.-X. Liu, D. J. Scalapino, and S.-C. Zhang, Phys. Rev. B **77**, 220503(R) (2008).
[28] E. Z. Kurmaev, J. J. Rehr, A. L. Ankudinov, L. D. Finkelstein, P. F. Karimov, and A. Moewes, J. Electron Spectrosc. Relat. Phenom. **148**, 1 (2005).
[29] A. Koitzsch *et al.*, Phys. Rev. B **78**, 180506(R) (2008).
[30] E. Z. Kurmaev, R. G. Wilks, A. Moewes, N. A. Skorikov, Y. A. Izyumov, L. D. Finkelstein, R. H. Li, and X. H. Chen, Phys. Rev. B **78**, 220503(R) (2008).
[31] D. A. Goodings and R. Harris, J. Phys. C **2**, 1808 (1969).
[32] E. Z. Kurmaev, R. G. Wilks, A. Moewes, L. D. Finkelstein, S. N. Shamin, and J. Kunes, Phys. Rev. B **77**, 165127 (2008).
[33] E. Z. Kurmaev *et al.*, J. Phys.: Condens. Matter **10**, 4081 (1998).